Received: 29 September 2022 | Accepted: 1 November 2022

DOI: 10.1002/pamm.202200043

A geometrical parameter study of the analytical stress calculation in adhesive joints with thick bonding layers

Thomas S. Methfessel[1,*] and **Wilfried Becker**[1]

[1] Technical University of Darmstadt, Institute of Structural Mechanics, Franziska-Braun-Straße 7, 64287 Darmstadt, Germany

Strength and failure analyses are critical to the safe and sustainable design of any structure. In the case of adhesively bonded joints, particular attention must be paid to the adhesive layer, which is comparably compliant and subject to high stresses. Determining the stresses in the adhesive layer is essential to identify critical areas in the joint and prevent the formation of cracks. In most applications, bonded joints have thin adhesive layers that can already be accounted for with highly simplified analytical models. However, for the consideration of thicker adhesive layers, advanced models are required that take the adhesive layer into account in more detail.

Therefore, in this work, an analytical model with a higher-order displacement approach is presented to account for more complex deformation behavior in the adhesive layer. The applied advanced displacement approach is particularly suitable for joints with thicker adhesive layers. In addition, the model enables the calculation of stresses and strains in bonded joints for a wide range of joint configurations and applications. A parameter study is carried out to evaluate the effect of different thicknesses of the adhesive layer and to show the advantages of the current model compared to other existing ones. For verification, all analytical results were compared with corresponding Finite Element Analyses.

1 Introduction

The evaluation of adhesive joints with finite element analysis shows a very high level of detail and accuracy of results. However, these numerical calculations are also accompanied by high computational effort and longer computing times. To speed up the evaluation and improve applicability, simplified analytical models can be used instead of complex finite element calculations. Volkerson [1] was the first to come up with an analytical model to predict stresses in bonded joints in 1938. The model, which was initially applied to riveted joints, could also be transferred to adhesive joints. The adhesive layer was regarded as a simplified continuum that could only transmit shear stresses between the joining partners. This model was extended in 1944 by Goland and Reissner [2], who evaluated stresses in cemented single-lap joints. The bonded parts (adherends) were treated as beams, which allow bending deformations that lead to a realistic determination of the transferred peeling stresses in the adhesive layer. This consideration is particularly important for single-lap joints. In later research work, these basic models were refined for different joint designs and configurations and different material properties. Some notable examples include the works of de Bruyne [3], Hart-Smith [4] and Srinivas [5], who analyzed joint configurations with beveled, scarfed, and stepped adherends. Wah [6] as well as Renton and Vinson [7] accounted for anisotropic adherends, applying laminate plate theory. Recently, Stein et al. [8] evaluated joints with functionally graded adhesive layers and Rosendahl et al. [9] investigated those with nonlinear adhesive layers.

In many of these models the so-called *general sandwich-type* approach is used, which was introduced by Bigwood and Crocombe [10] in 1989, and where only the overlap area, and not the entire joint, is modeled. This practical simplification enables the evaluation of many different joint designs and different load cases with only a single model. Regarding structures with thick adhesive layers, which are particularly addressed in this work, Ojalvo and Eidinoff [11] were the first to develop a model that takes greater account of the adhesive layer thickness by enabling a linear variation of the adhesive displacements in thickness direction. Based on the approach in this paper, the authors worked on further improved models to obtain more precise results. A first modification considering quadratic deformations in the adhesive layer was made in 2021 [12] followed by an even more advanced model published in 2022 [13] using higher-order approaches for the adhesive displacements. In this work, a parameter study is applied on the model of Methfessel and Becker [13] to examine and highlight its suitability for structures with thicker adhesive layers.

2 Analytical modeling of adhesive joints

The model presented below can be applied to various sandwich-type configurations with thicker and thinner adhesive layers. For simplicity and versatility, the structure is reduced to a two-dimensional system and the *general sandwich-type* approach [10] is applied. The single-lap joint shown in Fig. 1, is therefore reduced to the overlap region shown in Fig. 2, where the ends of

* Corresponding author: e-mail methfessel@fsm.tu-darmstadt.de, phone +49 6151 16-26145, fax +49 6151 16-26142

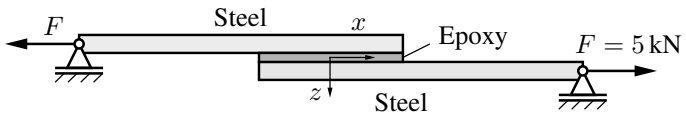

Fig. 1: Balanced *Steel - Epoxy - Steel* single-lap joint under tensile loading.

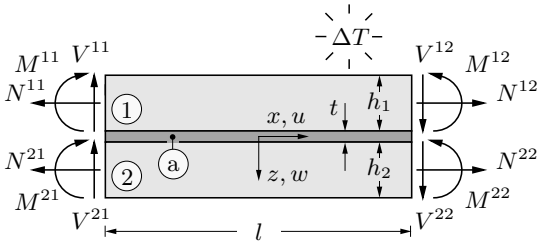

Fig. 2: General sandwich-type model of the joint.

the adherends and the external loads applied to them are introduced into the structure through sectional forces and moments. For uniform referencing, the indices 1 and 2 are introduced as notation for the upper and lower adherend and the index a is introduced for the adhesive layer. Considering the kinematics, the comparably stiff adherends are modeled as beams using first-order shear deformation theory:

$$u^{(i)}(x,z) = u_0^{(i)} + z\psi^{(i)}, \qquad w^{(i)}(x,z) = w_0^{(i)}. \tag{1}$$

The quantities u_0 and w_0, with the subscript zero, are the displacements of the horizontal centerline of the adherends and ψ denotes the rotation of their cross sections. The adhesive layer is modeled in a similar way to Ojalvo and Eidinoff [11], using a polynomial displacement approach. Instead of a linear distribution of the adhesive displacements in the thickness direction, we allow the model to capture linear, quadratic and cubic deformations:

$$u^{(\mathrm{a})}(x,z) = \frac{\hat{u}^{(1)} + \hat{u}^{(2)}}{2} + z\frac{\hat{u}^{(2)} - \hat{u}^{(1)}}{t} + \phi_{\mathrm{u}}(x)\mathcal{F}(z) + \chi_{\mathrm{u}}(x)\mathcal{G}(z), \tag{2}$$

$$w^{(\mathrm{a})}(x,z) = \frac{\hat{w}^{(1)} + \hat{w}^{(2)}}{2} + z\frac{\hat{w}^{(2)} - \hat{w}^{(1)}}{t} + \phi_{\mathrm{w}}(x)\mathcal{F}(z) + \chi_{\mathrm{w}}(x)\mathcal{G}(z). \tag{3}$$

Therefore, quadratic and cubic terms are added to the linear expressions to account for additional deformation modes. In Eqs. (2) and (3) the expressions $\hat{u}$ and $\hat{w}$ denote the adherends' displacements evaluated at their interfaces to the adhesive layer as functions of the coordinate x, given as:

$$\hat{u}^{(1)}(x) = u_0^{(1)}(x) + \frac{t}{2}\psi^{(1)}(x), \qquad \hat{w}^{(1)}(x) = w_0^{(1)}(x), \tag{4}$$

$$\hat{u}^{(2)}(x) = u_0^{(2)}(x) - \frac{t}{2}\psi^{(2)}(x), \qquad \hat{w}^{(2)}(x) = w_0^{(2)}(x). \tag{5}$$

The terms $\mathcal{F}(z)$ and $\mathcal{G}(z)$ in Eqs. (2) and (3) are quadratic and cubic functions of the coordinate z, multiplied by newly introduced deflection functions $\phi_{\mathrm{u}}(x)$, $\chi_{\mathrm{u}}(x)$, $\phi_{\mathrm{w}}(x)$ and $\chi_{\mathrm{w}}(x)$, representing quadratic and cubic deformation modes in the thickness direction. They are chosen as:

$$\mathcal{F}(z) = 1 - \frac{4}{t^2}z^2 \qquad \text{and} \qquad \mathcal{G}(z) = z - \frac{4}{t^2}z^3. \tag{6}$$

Assuming plane strain conditions for both the adherends and the adhesive layer, the displacements result in the following strains each:

$$\varepsilon_{xx} = \frac{\partial u}{\partial x}, \qquad \varepsilon_{zz} = \frac{\partial w}{\partial z}, \qquad \gamma_{xz} = \frac{\partial u}{\partial z} + \frac{\partial w}{\partial x}, \qquad \varepsilon_{yy} = \gamma_{yz} = \gamma_{xy} = 0. \tag{7}$$

Assuming linear elastic material behavior to the entire joint and beam theory to the adherends yields the constitutive equations

$$\begin{pmatrix}\sigma_{xx}\\ \tau_{xz}\end{pmatrix}^{(i)} = \begin{pmatrix}\frac{E}{1-\nu^2}\varepsilon_{xx} - \frac{E}{1-\nu}\alpha_T\Delta T\\ kG\gamma_{xz}\end{pmatrix}^{(i)}, \tag{8}$$

used in this work for the adherends as well as for the adhesive layer

$$\begin{pmatrix}\sigma_{xx}\\ \sigma_{yy}\\ \sigma_{zz}\\ \tau_{xz}\end{pmatrix}^{(a)} = E^{(a)^*}\begin{pmatrix}1-\nu & \nu & \nu & 0\\ \nu & 1-\nu & \nu & 0\\ \nu & \nu & 1-\nu & 0\\ 0 & 0 & 0 & \frac{1-2\nu}{2}\end{pmatrix}^{(a)}\begin{pmatrix}\varepsilon_{xx} - \alpha_T\Delta T\\ -\alpha_T\Delta T\\ \varepsilon_{zz} - \alpha_T\Delta T\\ \gamma_{xz}\end{pmatrix}^{(a)} \quad \text{with} \quad E^{(a)^*} = \frac{E^{(a)}}{(1+\nu^{(a)})(1-2\nu^{(a)})}. \tag{9}$$

As can be seen, thermal load cases are also considered in addition to purely mechanical ones.

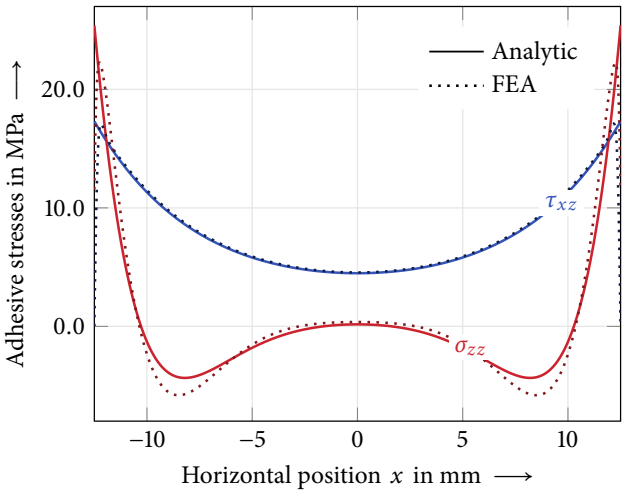

Fig. 3: Adhesive stress distributions along the horizontal centerline of a single-lap joint structure according to the analytic model by Ojalvo and Eidinoff and the numeric finite element analysis. The adhesive layer of the single-lap joint has a thickness of $t = 0.5\,\mathrm{mm}$.

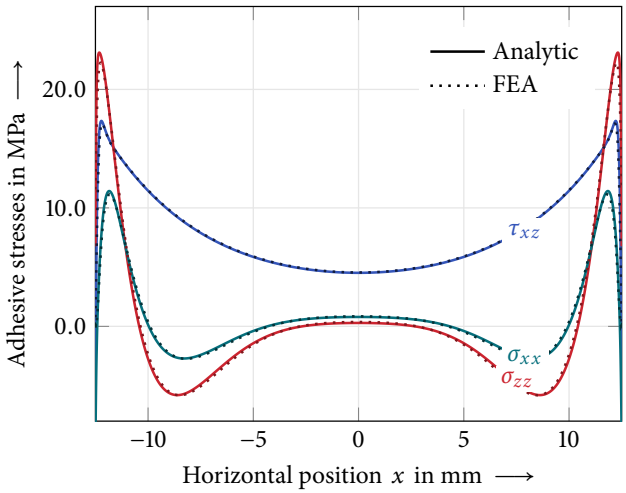

Fig. 4: Stress results of the single-lap joint structure with an adhesive thickness of $t = 0.5\,\mathrm{mm}$ calculated at the horizontal centerline at $z = 0\,\mathrm{mm}$. Analytical results from the present model are compared and verified with FEA.

With the expressions for stresses and strains, we can determine the total potential energy of the joint

$$\Pi = \Pi_\mathrm{i} + \Pi_\mathrm{a}, \tag{10}$$

which is composed of the internal potential energy Π_i, consisting of the strain energy, and the external potential energy Π_a, resulting from the external loading. The principle of minimum total potential energy is then applied to the total potential energy. Hence, the variation of the potential energy $\delta\Pi$ must vanish. Evaluating the equation

$$\delta\Pi \stackrel{!}{=} 0. \tag{11}$$

yields a second-order system of ordinary differential equations and boundary conditions depending on the introduced deflection quantities. To solve this system, it can be transformed into a first-order system of the form

$$\mathbf{A}\begin{pmatrix}\Psi\\ \Psi'\end{pmatrix}' + \mathbf{B}\begin{pmatrix}\Psi\\ \Psi'\end{pmatrix} = \mathbf{d}, \qquad \text{with} \qquad \Psi = \left(u_0^{(1)},\ u_0^{(2)},\ w_0^{(1)},\ w_0^{(2)},\ \psi^{(1)},\ \psi^{(2)},\ \phi_\mathrm{u},\ \chi_\mathrm{u},\ \phi_\mathrm{w},\ \chi_\mathrm{w}\right)^T. \tag{12}$$

The homogeneous part of the solution is obtained from the solution of an eigenvalue problem resulting from the application of the standard exponential solution approach. The eigenvalues determined in this process are a combination of real, complex, and zero eigenvalues. The particular part of the solution is calculated using a general constant approach. Further details on the analytical modeling can be found in the work of Methfessel and Becker [13] from 2022.

3 Results and discussion

To verify the implemented analytical model, comparative finite element analyses (FEA) were performed with ABAQUS and Python. For a direct comparison, only the overlap region was modeled, just as in the analytical model, and the system was reduced to a two-dimensional structure. Plane strain elements with quadratic shape functions were used in the meshing of the geometry, and refinements were made especially at the edges and in the adhesive layer, resulting in a mesh with approx. 40000 degrees of freedom. The analyzed structures in this paper are steel-epoxy-steel single-lap joints under mechanical tensile loading, as seen in Fig. 1. The investigated geometry in all diagrams has an overlap length of $l = 25\,\mathrm{mm}$, a structure depth of $w = 25\,\mathrm{mm}$ and adherend thicknesses of $h_1 = h_2 = 2\,\mathrm{mm}$. The adherends with a length of 50mm are loaded at the ends with mechanical tensile loads of $F = 5\,\mathrm{kN}$. For the given configuration and load case, we evaluated the occurring stress distributions in the adhesive layer and compared them with the results of Ojalvo and Eidinoff's model.

3.1 Model comparison

In Figs. 3 and 4 the same single-lap joint structure with an adhesive thickness of $t = 0.5\,\mathrm{mm}$ was analyzed. In both figures, the analytical and numerical stresses were evaluated along the horizontal centerline of the adhesive layer. The numerical results are from the finite element calculation, while the analytical results in Fig. 3 are based on Ojalvo and Eidinoff's already existing model and in Fig. 4 based on the present model. Comparing the analytical results of both diagrams, some differences in the

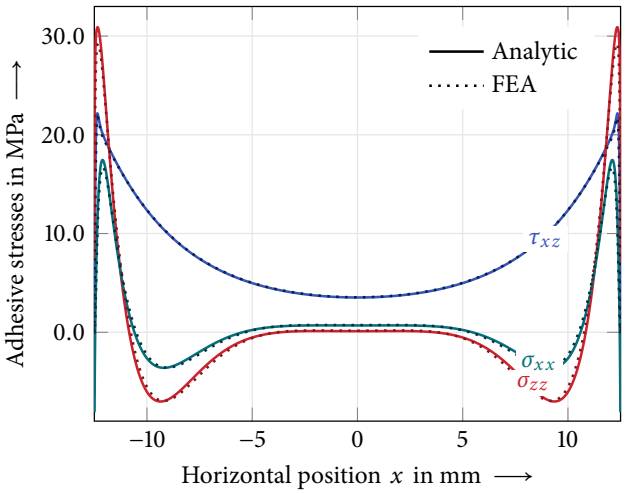

Fig. 5: Analytical and numerical stress results for a single-lap joint with a thinner adhesive layer of $t = 0.25\,\mathrm{mm}$. Evaluation path is the horizontal centerline of the joint.

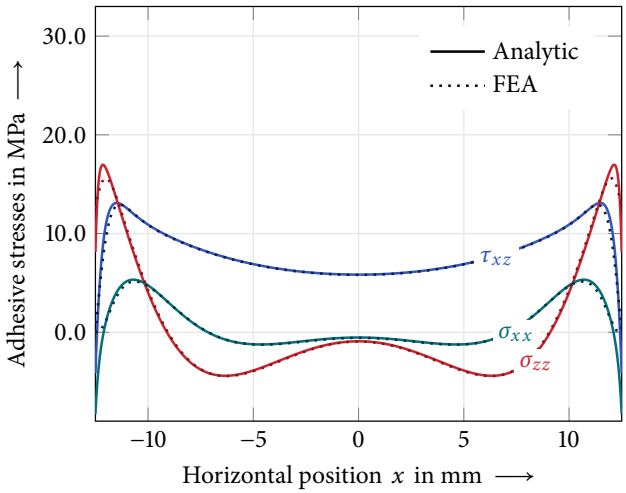

Fig. 6: Stress results for a thicker single-lap joint, with an adhesive thickness of $t = 2\,\mathrm{mm}$. Comparison of analytical and numerical results along the horizontal centerline of the joint.

stress distributions can be seen. Looking at the shear stresses, both models show mostly good agreement with the corresponding finite element results. However, only the present model predicts a stress reduction of the shear stresses at the ends of the adhesive layer, according to the stress-free edge condition. In the case of the peel stresses, the present model succeeds in a more accurate prediction, which is especially visible in the areas of the local peaks near $x = \pm 8\,\mathrm{mm}$. In addition to the shear and peel stresses the present model also gives the normal stresses in the direction of x. As can be seen, contrary to what was assumed in previous studies, they are not negligibly small.

3.2 Thickness comparison

Depending on the thickness of the adhesive layer, the resulting stress curves show very different results. In Figs. 5 and 6, a thinner single-lap joint with an adhesive layer thickness of $t = 0.25\,\mathrm{mm}$ and a thicker single-lap joint with an adhesive layer thickness of $t = 2\,\mathrm{mm}$ are compared. In both cases, the present model was applied to obtain the analytical results and the results show good agreement with the FEA. An interesting observation is that the stresses in the thinner structure in Fig. 5 show a much more localized behavior at the edge with higher stress concentrations than in the thicker structure. These high-edge effects caused by the load then subside very quickly towards the middle of the adhesive layer where a stress plateau with almost vanishing normal stresses is reached. The results of the thicker structure presented in Fig. 6 exhibit much smaller stress peaks and generally have a more even distribution along the horizontal centerline of the adhesive layer compared to the thinner structure.

In addition to evaluating the stresses along the horizontal mid-plane, we also look directly at the stress distributions through the thickness of the adhesive layer. Therefore, we have chosen a position x near the edge where the highest stresses occur according to the previous diagrams. According to the present model, the structure with the thinner adhesive layer in Fig. 7 shows approximately linear stress curves, which can also be determined by the linear approach suggested by Ojalvo and Eidinoff. However, the joint with a thicker adhesive layer shows a much more complex distribution, as shown in Fig. 8, which cannot be captured by a linear model. Thus, the present model succeeds in a good approximation of the FE results.

3.3 Parameter study

Finally, to further illustrate the suitability of this model for joints with thicker adhesive layers, the shear and peel stresses for the present model, the one by Ojalvo and Eidinoff and the FEA were evaluated at a specific point in the adhesive layer. As seen in Fig. 9 and 10, the thickness of the adhesive layer was continuously changed from very thin to thick and the effect on the resulting stresses was investigated. It can be seen, especially for the shear stresses in Fig. 9, that both analytical models give very good results for thin adhesive layers. However, as the thickness of the adhesive layer increases, Ojalvo and Eidinoff's solution deviates more from that of the current model and FEA. In contrast, the present model also continues to agree very well with the finite element results, even for thicker adhesive layers. Similar but slightly less precise findings can also be observed for the peel stresses in Fig. 10.

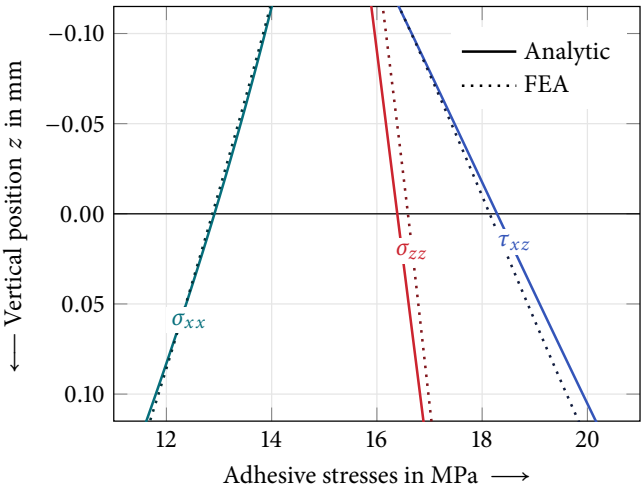

Fig. 7: Stress evaluation in thickness direction along a vertical path at $x = -11.75\,\mathrm{mm}$ for a single-lap joint with an adhesive thickness of $t = 0.25\,\mathrm{mm}$.

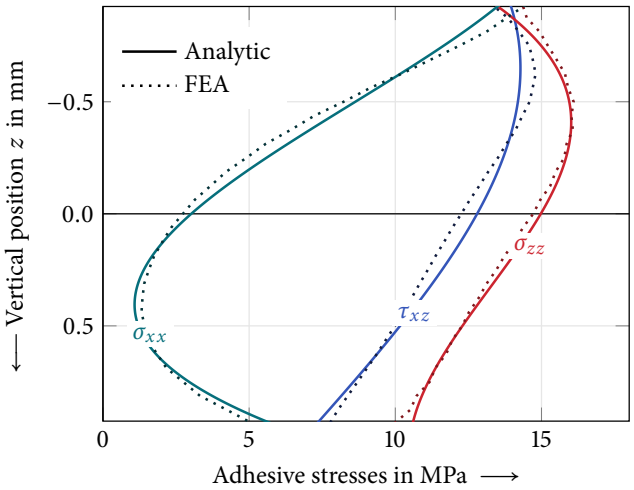

Fig. 8: Adhesive stress curves in through thickness direction at $x = -11.75\,\mathrm{mm}$ for a single-lap joint with an adhesive thickness of $t = 2\,\mathrm{mm}$.

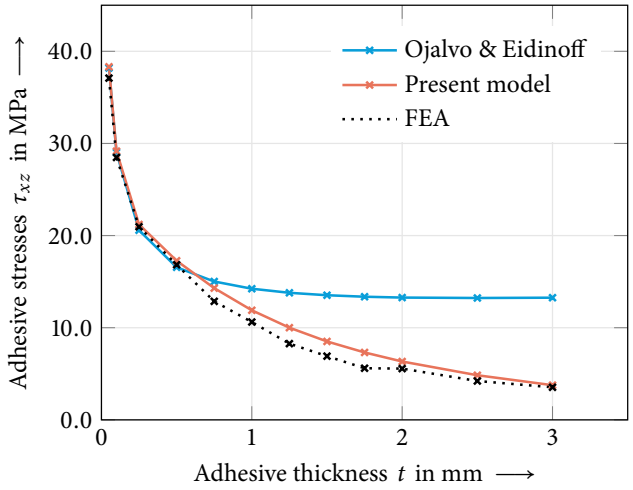

Fig. 9: Parametric study of the adhesive shear stresses evaluated at a specific point at $x = -12.25\,\mathrm{mm}$ and $z = 0\,\mathrm{mm}$ depending on the thickness of the adhesive layer. Comparison between the present model, the model of Ojalvo and Eidinoff and FEA.

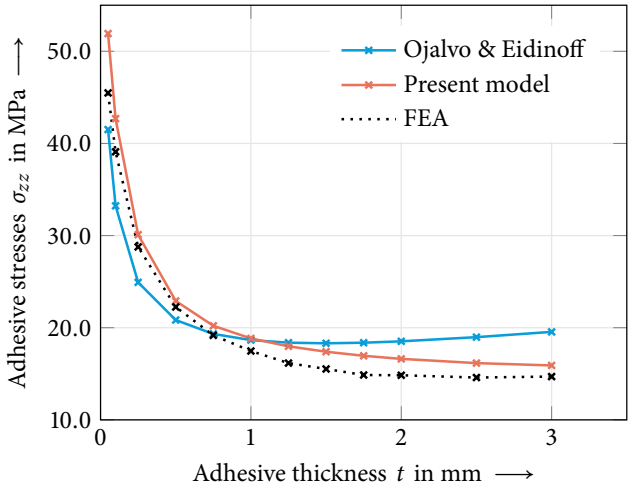

Fig. 10: The distribution of peel stresses for single-lap joints with different thicknesses. Comparison of the results from the present model, the model of Ojalvo and Eidinoff and FEA at $x = -12.25\,\mathrm{mm}$ and $z = 0\,\mathrm{mm}$.

4 Conclusion

In this work, a new, analytical calculation model is presented which, in addition to joints with thin adhesive layers, also provides rather accurate results for joints with thicker adhesive layers. The higher-order approach used allows a reasonably precise determination of the stresses in the adhesive layer. At the same time, the model is universally applicable, as different geometry and load configurations are covered. Finally, the analytical calculation procedure also provides all results very quickly.

Acknowledgements Open access funding enabled and organized by Projekt DEAL.

References

[1] O. Volkersen, Luftfahrtforschung **15**(1/2), 41–47 (1938).
[2] M. Goland and E. Reissner, J. Appl. Mech. **11**(1), A17–A27 (1944).
[3] N. A. de Bruyne, Aircl. Eng. Aerosp. Technol. **16**(4), 115–118 (1944).
[4] L. J. Hart-Smith, NASA, CR-112237 (1973).
[5] S. Srinivas, NASA, TN D-7855 (1975).
[6] T. Wah, J. Eng. Mater. Technol. **95**(3), 174–181 (1973).
[7] J. W. Renton and J. R. Vinson Eng. Fract. Mech. **7**(1), 41–52 (1975).
[8] N. Stein, P. Weißgraeber and W. Becker, Int. J. Solids. Struct. **97-98**, 300–311 (2016).

[9] P. L. Rosendahl, N. Stein and W. Becker, PAMM **17**(1), 341–342 (2017).
[10] D. A. Bigwood and A. D. Crocombe, Int. J. Adhes. Adhes. **9**(4), 229–242 (1989).
[11] I. U. Ojalvo and H. L. Eidinoff, AIAA Journal **16**(3), 204–211 (1978).
[12] T. S. Methfessel and W. Becker, PAMM **21**(1), e202100015 (2021).
[13] T. S. Methfessel and W. Becker, Compos. Struct. **291**, 115556 (2022).

